Dropping the hammer: Examining impact ignition and combustion using pre-stressed aluminum powder

Kevin J. Hill, Juliusz Warzywoda, Michelle L. Pantoya, and Valery I. Levitas

Citation: Journal of Applied Physics **122**, 125102 (2017); doi: 10.1063/1.5003632
View online: http://dx.doi.org/10.1063/1.5003632
View Table of Contents: http://aip.scitation.org/toc/jap/122/12
Published by the American Institute of Physics

Dropping the hammer: Examining impact ignition and combustion using pre-stressed aluminum powder

Kevin J. Hill,[1] Juliusz Warzywoda,[2] Michelle L. Pantoya,[1] and Valery I. Levitas[3,4]
[1]*Department of Mechanical Engineering, Texas Tech University, Lubbock, Texas 79409, USA*
[2]*Materials Characterization Center, Whitacre College of Engineering, Texas Tech University, Lubbock, Texas 79409, USA*
[3]*Departments of Aerospace Engineering, Mechanical Engineering, and Materials Science and Engineering, Iowa State University, Ames, Iowa 50011, USA*
[4]*Ames Laboratory, Division of Materials Science and Engineering, Ames, Iowa 50011, USA*

(Received 6 September 2017; accepted 7 September 2017; published online 22 September 2017)

Pre-stressing aluminum (Al) particles by annealing and quenching Al powder alters particle mechanical properties and has also been linked to an increase in particle reactivity. Specifically, energy propagation in composites consisting of aluminum mixed with copper oxide (Al + CuO) exhibits a 24% increase in flame speed when using pre-stressed aluminum (PS Al) compared to Al of the same particle size. However, no data exist for the reactivity of PS Al powders under impact loading. In this study, a drop weight impact tester with pressure cell was designed and built to examine impact ignition sensitivity and combustion of PS Al when mixed with CuO. Both micron and nanometer scale powders (i.e., μAl and nAl, respectively) were pre-stressed, then combined with CuO and analyzed. Three types of ignition and combustion events were identified: ignition with complete combustion, ignition with incomplete combustion, and no ignition or combustion. The PS nAl + CuO demonstrated a lower impact ignition energy threshold for complete combustion, differing from nAl + CuO samples by more than 3.5 J/mg. The PS nAl + CuO also demonstrated significantly more complete combustion as evidenced by pressure history data during ignition and combustion. Additional material characterization provides insight on hot spot formation in the incomplete combustion samples. The most probable reasons for higher impact-induced reactivity of pre-stressed particles include (a) delayed but more intense fracture of the pre-stressed alumina shell due to release of energy of internal stresses during fracture and (b) detachment of the shell from the core during impact due to high tensile stresses in the Al core leading to much more pronounced fracture of unsupported shells and easy access of oxygen to the Al core. The μAl + CuO composites did not ignite, even under pre-stressed conditions. *Published by AIP Publishing.*
[http://dx.doi.org/10.1063/1.5003632]

I. INTRODUCTION

Aluminum powder is a metal fuel used in a variety of energy generating composites. With 85 GJ/m^3 of energy available from the oxidation of Al to Al_2O_3, aluminum offers increased energy density when compared to organic energetic materials. However, much of the potential chemical energy stored within an Al particle is never harnessed due to incomplete combustion or poor oxidation reaction kinetics. Also, Al oxidation is limited by an Al_2O_3 passivation layer that surrounds an Al particle, slows reaction rates, and can reduce total energy generation.

We have studied an approach to enhancing the reactivity of Al powder by pre-stressing Al powder using annealing and quenching treatments. Based on the melt-dispersion mechanism,[1,2] Levitas *et al.* suggested that producing internal compressive stresses in an oxide shell should increase Al particles reactivity. Compressive stresses in a shell delay its fracture during fast heating and increase the amount of Al melt required to break a shell. The larger amount of Al melt, which disperses into small droplets after shell fracture and reacts on the time scale of flame front propagation, increases flame speed and, consequently, Al reactivity. It was suggested in Ref. 1 that annealing the Al particle to a higher temperature should produce and then relax internal thermal stresses due to the difference in thermal expansion between Al and alumina. Relaxation of internal stresses changes the stress-free temperature of the Al core–alumina shell structure to the annealing temperature. As the particles cool down to room temperature, internal thermal stresses of the opposite sign (compressive in the shell and tensile in the core) should appear. Fast quenching rates are required to avoid relaxation of these induced internal stresses. This prediction was experimentally confirmed in Levitas *et al.*:[3,4] for annealing temperature in the range of 105–200 °C, the flame propagation speed for Al nano- and micron-scale particles was increased by 30%–40%. Note that these numbers were in quantitative agreement with theoretical predictions based on the melt dispersion mechanism.[1,2] Similar results on increased reactivity were obtained in McCollum *et al.*[5] In particular, they found pre-stressed (PS) Al powder annealed at or above 300 °C showed the highest increase in reactivity.

In later works, Levitas *et al.*[6] and McCollum *et al.*[7] performed Synchrotron XRD (X-ray diffraction) measurements on 5 μm average diameter Al particles to determine dilatational strain in the Al core before and after annealing and

quenching. They determined that particles annealed to 300 °C demonstrated (in contrast to pristine particles) significant dilatational strain, which corresponds to compressive stress in the alumina shell and tensile stress in the core. This finding was conceptual and quantitative proof that the improvement of Al reactivity is related to internal stresses. The dilatational strain is the key measurable parameter that allows one to characterize internal stresses in pre-stressed particles. Pre-stressed Al particles exhibited 32% (Ref. 6) and 24% (Ref. 7) increase in flame speed over untreated particles when mixed with copper oxide. Stress relaxation during storage of Al particles was also studied experimentally and theoretically in Ref. 8.

Aluminum particles that are added to consolidated composites and subjected to high-velocity impact ignition can provide a secondary blast effect but often do not significantly contribute to the energy generated in the initial blast wave.[9–11] Aluminum particles, especially in the micron scale size range, simply are too big to react at the time scales of the initial compressive wave associated with kinetically controlled reactions from organic explosives. After the initial shock wave heating, aluminum disperses in the fragmented debris of the reactive composite and participates in releasing chemical energy via oxidation reactions. Aluminum reacting under these conditions provides an enhanced blast effect by increasing the energy output after the initial blast wave but does not contribute to energy released in the shock wave. In Ref. 12, high velocity impact ignition of aluminum composite reactive materials showed fracture behavior (governed by composite strength) affected fragmentation upon impact. They observed that smaller fragments upon impact resulted in greater overall reactivity. One approach to increasing the Al reactivity upon impact and thereby increasing the reactivity of the composite is to alter the mechanical properties of the Al particle that may also affect fragmentation and the corresponding ignition mechanism. For example, Bachmair and Pippen[13] showed that Al powder in the micron size range exhibits considerable changes in mechanical properties, and particularly that grain growth and softening both occur for Al powders when annealed at or above 300 °C. Hardness of the Al powder consolidated into pellets reduced by ∼10% after annealing at 300 °C. This altered mechanical property is hypothesized to affect fragmentation as well as hot spot formation. Smaller fragmentations should correlate with increased energy generation. Ideally, a greater chemical energy release in the initial blast that could be garnered through aluminum particle combustion would transform impact ignition events. Towards this end, efforts on altering the mechanical properties of Al particles may induce alternative reaction mechanisms and promote Al reactivity under impact.

As a step towards this goal, the objective of many studies has been to investigate low-velocity, or drop-weight impact ignition on small, laboratory-scale samples to assess the feasibility of various approaches towards enhancing Al (or other metal fuel particle) reactivity under impact loading. Initial work focused on: (1) understanding the role of the oxidizer in an Al composite during impact ignition;[14] (2) increasing the mechanical strength of the overall composite;[15] and (3) adding high friction components like silica to the composite to increase frictional heating.[16] While changing oxidizers alters combustion chemistry, both increasing mechanical strength and adding high friction components attempt to increase hot spot formation through mechanical processes in the composite to reduce impact ignition energy threshold. Increasing the mechanical strength leads to more energy consumption during plastic flow upon impact, and high friction components create hot spots through an interfacial friction between particles during initial deformation upon impact. In fact, Hardt[16] and Davis and Woody[17] showed that localized heating leading to ignition under impact conditions can occur due to friction between moving particles; and, initiation of local chemical reactions through particle collisions. These previous studies indicate improving hot spot formation is a primary mechanism for improving ignition sensitivity for aluminum composites under impact. They also demonstrated that mechanical properties such as strength and brittleness[18] can increase hot spot formation. Annealing and quenching, due to the effects of pre-stressing, may maximize the effect of hot spot formation by increasing the strength of the shell and local stresses. Reduced hardness of Al particles due to annealing may lead to stronger strain localization upon impact and increase hot spot formation through heat build-up during deformation.[19] It is also possible that, due to the residual compressive stress in the alumina shells after annealing and quenching, the thin shell is more susceptible to delamination and spalling from the core upon impact,[20] leading to increased Al exposure to oxygen.

Investigations of impact ignition sensitivity of aluminum with metal oxide composites have not included studies focused on pre-stressed Al particles, and this work attempts to address this gap. While much work has been pursued to improve Al reactivity under impact, such work is, in many ways, dependent on the drop-weight impact tester. Generally, the energy of the impacting weight is the primary parameter used to understand and control ignition, with Ref. 21 showing a linear dependence of ignition on impact energy. Several drop-hammer testing apparatuses exist, though they differ primarily in how they constrain the sample and in the mass of the impactor.[22] They also differ in how they characterize ignition. While all drop-weight impact systems use some form of "go, no-go" tests, where the sample either reacts (a "go") or does not (a "no-go"), a "go" criteria can range from first light detected to discoloration or gas release.[23] Laboratory scale instruments have been constructed with glass anvils to mitigate this problem, and high speed photography as well as infrared photography have been employed to observe reactions.[24] Although each drop-weight impact apparatus offers a generally qualitative view of impact sensitivity due to differences in stiffness and machining tolerances, they are exceptionally useful in characterizing materials and studying ignition mechanisms.[25] It is important to note that for reactions occurring at very high rates (such as detonation of high explosives), an accurate view of impact ignition requires minimization of stored elastic energy in the impact tester itself.[26] However, in this work studying powder mixtures, the reaction speeds are much slower than with explosives, and ignition occurs well after the impact event is complete. This work presents a drop-weight impact tester capable of measuring

instances of first light as well as reaction completeness in terms of transient pressure and photodiode sensors.

The goal of this study is to optimize Al reactivity under impact ignition and specifically focus on low-velocity, drop-weight impact ignition. The objectives are to treat aluminum powder with prescribed annealing and quenching routines and examine Al + CuO composites under impact ignition for untreated as well pre-stressed Al powder. A second objective is to introduce an impact ignition apparatus that enables characterization of ignition and subsequent reaction to evaluate the effect of pre-stressed Al + CuO composites compared to their untreated counterparts. Both micron and nanometer scale Al particles are examined and material preparation and characterization was accomplished using established protocols.[5] Impact ignition analyses were accomplished by designing a pressurized reaction cell coupled with a traditional drop weight impact tester. The pressurized reaction cell is equipped with sensors to monitor the transient pressure and light intensity within the closed cell upon sample impact. In this way, both ignition and the subsequent combustion event were examined.

II. EXPERIMENTAL

A. Aluminum pre-stressing

Nano-aluminum (nAl) powder with an 80 nm average particle diameter was supplied by Novacentrix (Austin, TX), and 3–4.5 μm aluminum (μAl) powder was supplied by Alfa Aesar (Ward Hill, MA). Both powders have spherical particles with a ~4 nm amorphous aluminum oxide shell that inherently passivates the aluminum core from spontaneous reaction with oxygen in the environment. In supplementary material, Fig. S1 shows a transmission electron microscope (TEM) image of a representative Al nano-particle illustrating the core-shell microstructure. The nAl powder consists of about 80 wt. % Al and 20 wt. % Al_2O_3, and the micron powder is about 98 wt. % Al and 2 wt. % Al_2O_3.

All pre-stressed aluminum (PS Al) powders were heat treated in a controlled thermal environment using a Q800 DMA (Dynamic Mechanical Analyzer) from TA Instruments. Heating was performed in an air atmosphere at a heating rate of 10° C per minute to 300 °C and held for 15 min. Cooling with liquid nitrogen was programmed at an exponential rate to 25 °C according to Eq. (1) with $A = 0.0078\ s^{-1}$, $T_a = 25$, $T_0 = 300$, and t is time in seconds.

$$T = T_a + (T_0 - T_a)\exp(-At). \quad (1)$$

Equation (1) models lumped capacitance cooling and a graphic showing the heating and quenching cycle is provided in the supplementary material, Fig. S2.

B. Mixture preparation

Mixtures with pre-stressed aluminum (PS Al), along with untreated aluminum (Al), were mixed with spherical 50 nm average diameter copper oxide (CuO) particles from Sigma Aldrich (St. Louis, MO) at an equivalence ratio of 1.3, and all samples were prepared for this stoichiometry. Microstructure of the mixture is shown in supplementary material, Fig. S3.

Aluminum and copper oxide mixing was carried out with an acetone carrier fluid. For example, 134 mg of nAl combined with 365 mg of CuO were added to 50 ml of acetone and mixed using a sonic mixer (Misonix Sonicator 3000) for 2 min in a programmed cycle of 10 s on/off to prevent thermal energy buildup during mixing. All mixtures were prepared using the same procedure. The suspensions were placed in a Pyrex® dish and allowed to dry for 24 h in a fume hood. Upon retrieval, all samples were sieved through 325 mesh using a grounded brush to break up any large agglomerations in the powder. The powder mixtures were immediately available for further experimentation.

C. Drop weight impact tester

The drop impact tester is pictured in Fig. 1(a) and consists of two main components: the striker frame and the pressure cell. The striker frame consists of a 38 mm 80/20 aluminum frame that rigidly aligns two 12.7 mm diameter guide rails vertically and parallel. This entire assembly mounts to a steel C-channel, keeping the frame upright and allowing for height graduations consisting of holes drilled in the C-channel. The impact is carried out by a carriage that rides on ball bearing pillow blocks running along the guide rails. The carriage is modular, allowing for increases in

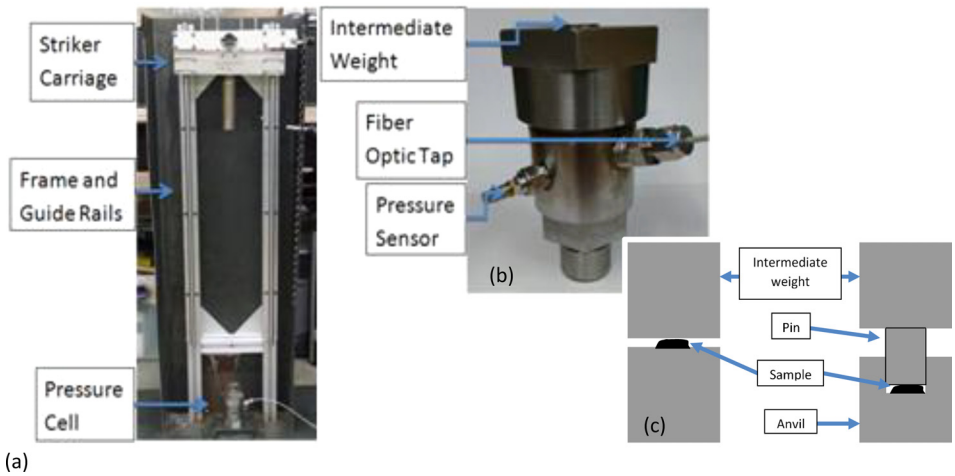

FIG. 1. (a) Photograph of the drop weight impact testing apparatus including striker carriage, frame and guide rails and pressure cell (0.6 m total maximum drop distance); (b) photograph of pressure cell portion of the drop weight impact tester illustrating sensor instrumentation; and (c) schematic of the Taylor rod-on-anvil setup vs. radially constrained anvil setup.

mass, from 1.5 to 6.2 kg, and pillow block replacement. A steel striking face is attached to the carriage. This face strikes against an intermediate weight inside the pressure cell and transfers energy to the sample. The maximum energy that can be delivered by the striker carriage is 42 J (Fig. S4, supplementary material). It is also possible to tune impact velocity while maintaining impact energy at energies below the maximum. This impact tester has two different anvils [Fig. 1(c)]. The first is a modified Taylor rod-on-anvil type, and the sample material is able to flow outward upon impact. The second anvil is radially constrained, consisting of a 6.35 mm diameter hole bored in a steel anvil with a pin that compresses the powder upon impact.

Instrumentation for characterizing a sample reaction includes a high speed camera (Phantom v2512), a photodiode, and a pressure sensor (PCB 101A06). The high speed camera is used to determine the impact velocity. The photodiode embedded in the pressure cell "sees" the reaction through a fiber optic cable and enables a "go, no-go" characterization of the ignition event. The pressure sensor records a pressure-time history within the cell [Fig. 1(b)], and is modular, allowing the use of dynamic or static pressure sensors. The sensors interface with a National Instruments cDAQ-9172 using 9215 cards. Data can be recorded at 100 000 samples per second per channel. A Matlab R2015a academic license code triggers the high speed camera, synchronizes collected data, stores the data for future use, and displays the data graphically for a quick assessment of the ignition event.

Tests using the high speed camera with a pixel to distance calibration were performed to determine impact velocity from a fixed height using various masses. The results showed that for a 1.5 kg carriage mass, the average impact velocity measured 1.87 m/s while at 6 kg, the average impact velocity measured 1.91 m/s. Both measurements exhibited a standard deviation of +0.01 m/s such that the impact velocity was constant over a range of masses. This indicates that friction along the guide rails is not relevant at low carriage masses and velocity is insensitive to carriage mass.

D. Experimental setup

Samples were loaded into the pressure cell using a low friction polymer plunger to eliminate sample loss through sticking to the plunger. Using the rod-on-anvil setup, the final powder measured 1 mm in diameter by 1 mm high with a mass of 10 mg. These samples were placed in the center of the anvil in the pressure cell, and an intermediate weight was placed on top. Using the radially constrained setup, the final powder fully covered the bottom of 6.35 mm diameter hole with a thickness of 1 mm and a mass of 20 mg (10 mg did not consistently cover the full bottom of the hole). The carriage height was set, and a pull pin was employed to drop the carriage down the rails. No carriage catch was utilized because the pressure sensor and high speed camera (triggered simultaneously) can determine the moments when the carriage strikes the intermediate weight. Multiple heights, weights, and sample masses were tested to determine the energy level that would cause ignition, and this approach is called the Bruceton method. The energy level is increased or decreased based on the results of the previous impact experiments (how many ignition events occur), and the ignition threshold is defined as the level at which one sample in 10 ignites. Light emission and pressure data were gathered for all of these tests, along with a high speed video of the falling carriage to determine impact velocity.

E. Product characterization

After the impact tests, select samples were placed in a Hitachi S-4300 scanning electron microscope (SEM) equipped with an EDAX energy dispersive X-ray spectrometer (EDS) for imaging and to obtain elemental maps, respectively. Pre-stressed and untreated aluminum particles that were impacted were also imaged using a Hitachi H-9500 transmission electron microscope (TEM) to examine the morphological structure at the core-shell interface.

III. RESULTS

A. Impact ignition

The samples demonstrated three different responses to impact that are shown in Fig. 2 for nAl + CuO representative mixtures. Figure 2 shows pressure and photodiode (i.e., light intensity) signals as a function of time for each type of response. Figure 2(a) shows no ignition and a complete lack of reaction, referred to as "no ignition and no reaction." In Fig. 2(b), the sample is consumed during combustion, and this case is referred to as "ignition and compete reaction." In Fig. 2(c), the sample began to ignite, but the reaction quenched before the sample was completely consumed, and this case is

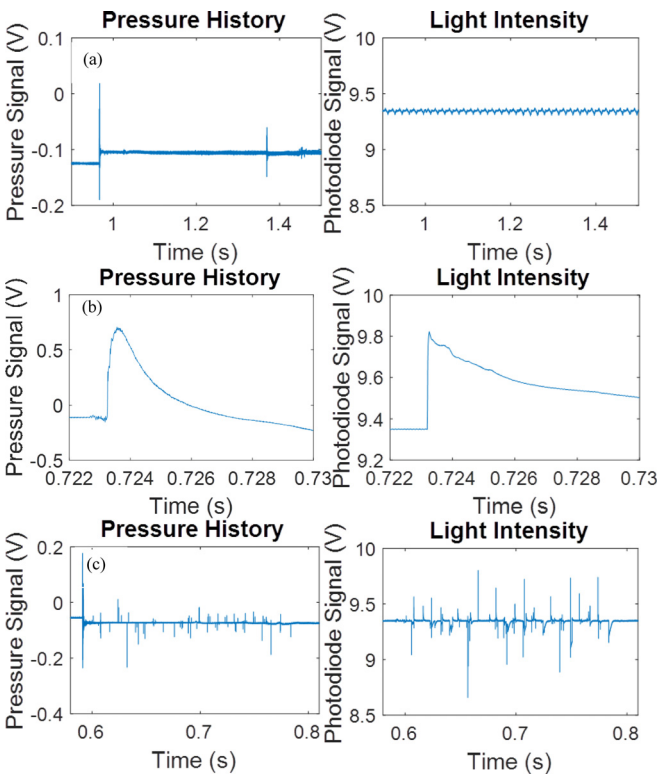

FIG. 2. Pressure and photodiode signal as a function of time for (a) no ignition and no reaction; (b) ignition and complete reaction; and (c) ignition and partial reaction.

TABLE I. Minimum energy required (E_{ign}) for complete and incomplete combustion for both pre-stressed (PS) and untreated nAl + CuO samples and for both anvil types.

Anvil type	Material	E_{ign} complete combustion (J/mg)	E_{ign} incomplete combustion (J/mg)
Taylor rod-on-anvil	PS nAl + CuO	0.7	0.07
Taylor rod-on-anvil	nAl + CuO	4.2	0.12
Radially constrained anvil	PS nAl + CuO	N/A	0.07
Radially constrained anvil	nAl + CuO	N/A	0.34

referred to as "ignition and partial reaction." It is noted that in Fig. 2(b), complete combustion may not have occurred (some unreacted Al may still exist), but the result is that the sample more completely reacted than in Fig. 2(c), and thus will be referred to as complete combustion.

Table I shows the minimum energy levels required for both complete and incomplete combustion events using the Bruceton method. The ignition threshold is defined as the energy level at which incomplete combustion first occurs. This is significant because this energy level is also the energy level at which light and pressure increases can first be observed. It should be noted that all μAl + CuO and PS μAl + CuO did not react at any available energy level and thus all ignition results shown in Table I are for nAl mixtures only.

B. Combustion completeness

Further analysis focuses on the nAl + CuO mixtures using Taylor rod-on-anvil configuration because this configuration also produced complete combustion events. Figure 3 shows pre-stressed vs. untreated nAl + CuO pressure histories for the ignition and complete combustion case. The comparison enables observation of the effect that pre-stressed nAl has on combustion of the impacted reactants. Higher peak pressures, as well as increased pressurization rate and energy generated (measured from the area under the pressure time curves), are clearly observed for the PS nAl + CuO. Also interesting is the longer duration of pressure decrease

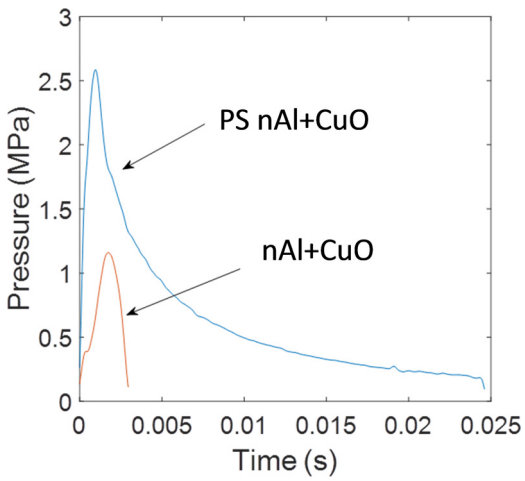

FIG. 3. Comparative pressurization curves for pre-stressed (7 J) vs. untreated (42 J) nAl + CuO mixtures.

associated with PS nAl + CuO as opposed to the nearly immediate drop in pressure for nAl + CuO. Data comparing the distinct pressure responses for the two samples are shown in Table II.

The pressure sensor voltage peaks in Fig. 2(a) are from the carriage impact only. The pressure sensor and photodiode voltage peaks in Fig. 2(b) are characteristic of combustion. Finally, Fig. 2(c) demonstrates incomplete combustion. While it is clear that some hotspots formed and were visible both to the pressure sensor and the photodiode in Fig. 2(c), the curves do not demonstrate a clear pressurization event or sensor (photodiode and pressure) voltage decay. An apt description is that the samples "fizzled" rather than burned completely.

Figures 4(a) and 4(b) show a photograph of the Taylor rod-on-anvil setup and intermediate weight after complete combustion and a photograph of a pellet that did not react completely, respectively. Figure 4(a) shows condensed copper on the anvil and intermediate weight and no pellet remaining. Figure 4(b) shows darkened edges that began to react but quenched for a sample that did not react completely. This sample also demonstrates that burning begins at the edges of the sample.

To demonstrate that hot spots were indeed formed in the incomplete combustion cases, SEM images coupled with EDS elemental maps of samples after the impact were taken. Figure 5 shows particles in a hot spot with a considerably larger size and different morphology compared to those for the reactant particles. Figure 5(a) shows larger grain-like structures surrounded by much smaller spherical particles. These grains are likely metallic copper grains that are formed in a hot spot. Figure 5(b) shows EDS elemental maps for a similar structure. The EDS analysis shows that the grain-like structures are likely made of copper, indicating that a hot spot is formed.

Table I indicates that first light is a poor way to define ignition, and that ignition is clearly distinct from the degree of combustion completeness. First light corresponds to the first instance of hot spot formation, which is not indicative of reaction propagation and overall reactivity. It is, however, a useful measure to determine the energy threshold required to locally ignite reactive mixtures, defining safe handling levels. It also provides insight into initiation mechanisms, like hot spot formation and adiabatic pore collapse.

To further investigate completeness of combustion, the pressure curves (Fig. 3) obtained for both untreated and pre-stressed nAl particle mixtures were numerically integrated to examine gas generation, which in turn relates to the amount of material consumed during combustion. The integral value

TABLE II. Peak pressure, pressure curve area, and pressurization rate data for pre-stressed vs. untreated nAl + CuO mixtures for the Taylor rod-on-anvil setup.

Material	Peak pressure (MPa)	Pressure curve area (kPa·s)	Pressurization rate (MPa/ms)
PS nAl + CuO	2.58	19.6	2.42
nAl + CuO	1.16	2.1	0.58

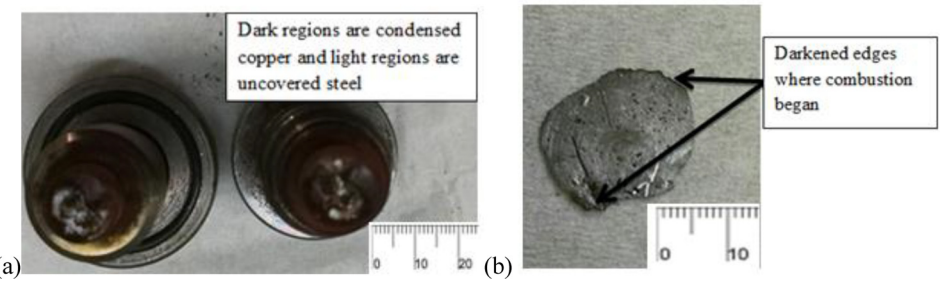

FIG. 4. (a) Anvil and intermediate weight after complete combustion (scale in mm); and (b) powders form a consolidated pellet after incomplete combustion (scale in mm). Photograph in (b) shows blackened areas corresponding to regions of the reacted material (i.e., localized hot spots).

of the pressure curve for the pre-stressed nAl particles was 833% higher than for untreated nAl particles (Table II). Figure 3 also demonstrates significantly higher peak pressure associated with pre-stressed nAl particles (123% higher than for untreated nAl particles, Table II). Pressurization rates also significantly increased from 0.58 MPa/ms (untreated) to 2.42 MPa/ms (pre-stressed), a 317% increase (Table II). These values show that pre-stressed particles experience significantly more complete reactions in addition to initiating at lower energy levels.

Possible mechanisms responsible for the effect of pre-stressing on ignition and combustion behavior are discussed. Changes in mechanical properties of Al[12] are too modest to cause the strong effects documented earlier. The melt-dispersion mechanism requires virtually perfect shells; however, impact loading damages the shells, which makes the melt-dispersion mechanism improbable.

Annealing and quenching changes the temperature T_0 at which the core-shell system is stress-free. In Ref. 4, for the same Al nanoparticles as here, changing T_0 from 25 to 105 and 170 °C changed the pressure in a core from −0.08 GPa (compressive) to 0.04 and 0.14 GPa (tensile) and the hoop stress in a shell from −0.19 GPa, to −0.74 GPA and −1.20 GPa, respectively. These numbers have been obtained using elasticity theory equations presented in Ref. 4 and they were in good agreement with results on flame speed measurements in Ref. 4 based on the model connecting flame propagation speed and stresses in particles. This model has multiple experimental confirmations for nanoparticles[1,2,4,27] and microscale particles.[1–4,28,29] In addition, the same elasticity theory equations are in good agreement with measurement of strains in the Al core shown in Refs. 5–8 for micron scale particles. Based on these equations, annealing at 300 °C should lead to the tensile mean stress in a core of 0.33 GPa and the hoop stress in a shell of −2.08 GPa, respectively.

Without external loading, compressive hoop stresses in a shell suppress fracture of the shell due to tensile hoop stresses produced during thermal expansion and melting of the core. At the initial stage of impact, local contact loading of some regions of the shell causes local bending and fracture of the shell, exposing the bare core, which starts reacting with gaseous oxygen or oxygen from CuO. Small bare core regions may heal during oxidation without producing a self-supporting reaction. The larger the bare area, the larger the chances that a reaction will be pronounced enough to be detected as an ignition event. For some critical bare area, the reaction will continue self-propagating without quenching until completion. Since the reaction is diffusion driven, smaller particles with a larger surface area to volume ratios will promote greater particle reactivity. This is a traditional argument that explains much higher reactivity of nanoparticles versus micron scale particles. For nanoparticles, compressive hoop stresses in the shell should delay fracture of the shell due to bending from larger contact stresses. However, since internal stresses accumulate elastic energy, which is released during fracture, and since larger compressive stresses in thin films lead to greater energy release rates upon fracture,[30] fracture may be more pronounced, producing larger bare areas of Al. Additionally, due to the softening of the aluminum, coupled with the increased fracture and large plastic deformations during impact, Al may be extruded through the cracks in the shell, increasing contact with oxygen.[31] Furthermore, large tensile stresses in the Al core and, consequently, at the aluminum-alumina interface, may cause decohesion at the interface during impact, leaving unsupported shells. This drastically increases the area of the Al core accessible by gaseous oxygen and reduces shell strength under load. These differences may explain significantly lower impact energy for ignition and completion of reaction of pre-stressed Al in comparison with untreated Al. These two mechanisms are illustrated in Fig. 6.

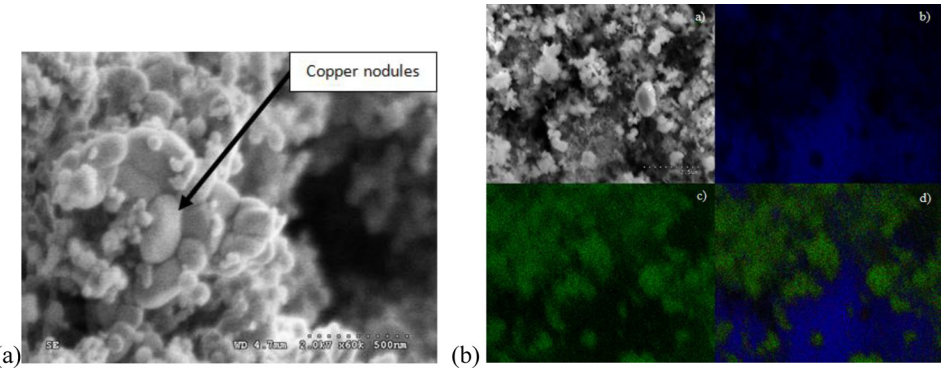

FIG. 5. (a) SEM image showing structures that appear to be copper nodules in a hot spot after impact. (b) Another SEM image (a) of nodules with corresponding EDS maps of (b) Al (blue), (c) Cu (green), and (d) a composite EDS map of Al and Cu.

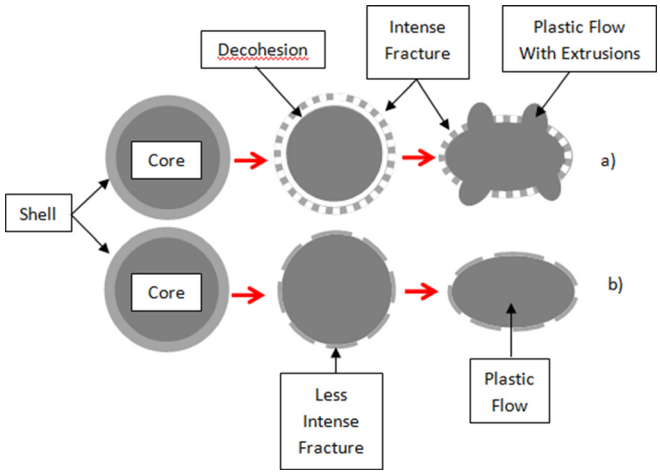

FIG. 6. Series (a) Pre-stressed aluminum under impact, Series (b) untreated aluminum under impact.

The proposed reaction mechanism is further supported by TEM imaging. Nanoparticle aluminum samples (both pre-stressed and untreated) were impacted at 4.2 J/mg and imaged using a TEM at 300 kV. These samples did not contain CuO, but instead this experiment was purposefully designed to examine Al particles under impact conditions. These experiments were performed in an air environment and immediately imaged proceeding their impact. Figure 7(a) shows a bulge at the interface between the darker core and lighter shell portion of the particle that could be indicative of extrusion behavior.

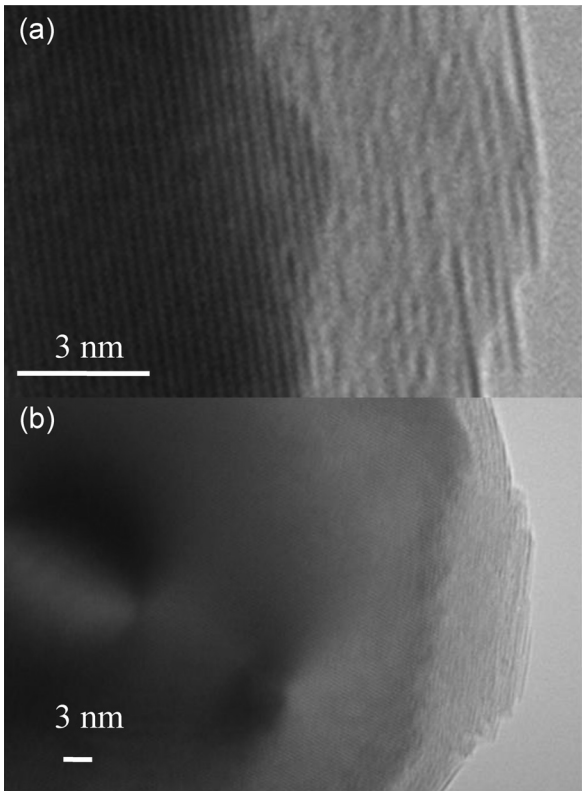

FIG. 7. TEM images illustrating possible mechanisms promoting impact ignition and reaction in pre-stressed nAl particles. (a) TEM image showing extrusion phenomena and (b) TEM image showing shell buckling in pre-stressed nAl particles.

An exposed surface may have had time to heal within the air environment but Fig. 7(a) suggests some plastic flow resulting from the impact event. Figure 7(b) demonstrates shell buckling may be possible. Significant damage to the shell is not apparent because these particles were impacted in an ambient environment, such that shell healing could have occurred quickly.

The difference in the impact energy between unconstrained and radially constrained loading can be explained as follows. For constrained loading, the mass of the powder does not reduce, and deformation represents compaction with small radial sliding along the anvil. The main heat sources are distributed along the multiple contact surfaces between particles due to contact friction producing hot spots. During unconstrained loading, a major part of the reactive mixture flows outside the anvils due to radial flow, which effectively increases supplied energy per unit mass. There is large relative displacement of particles with respect to the anvil's surface, causing large shear strain and more intense shell fracture and localized surface heating. Detached shells of the pre-stressed particles break much easier than those attached to the core shells of the untreated particles. This explains the much lower impact energy required for complete combustion of the pre-stressed particles when compared to untreated particles. The fact that the same impact energy required for ignition of pre-stressed particles for constrained and unconstrained loadings means that for such small impact energies, radial displacements are not pronounced.

IV. CONCLUSION

A low velocity impact tester was designed and used to characterize the ignition and combustion response of aluminum and copper oxide (Al + CuO) composites. The results show that pre-stressing (PS) aluminum powder with a prescribed annealing and quenching treatment leads to 3.5 J/mg difference in complete combustion threshold and a 0.05 J/mg difference in ignition threshold for PS nAl + CuO mixtures compared to their untreated counterpart when using a Taylor rod-on-anvil setup. The difference in ignition threshold when using a radially constrained anvil was even larger, at 0.27 J/mg. Complete combustion results using the Taylor rod-on-anvil setup showed that the area under the pressure curves was increased by an average of 833%, indicating a large increase in gas generation and combustion completeness. Peak pressure and pressurization rate were also increased dramatically via pre-stressing (123% and 317%, respectively). The most probable reasons include (a) delayed but more intense fracture of the pre-stressed alumina shell due to release of energy of internal stresses during fracture and (b) detachment of the shell from the core during impact due to high tensile stresses in an Al core leading to a much more pronounced fracture of unsupported shells and easy access of oxygen to the core.

SUPPLEMENTARY MATERIAL

See the supplementary material for TEM and SEM analysis of the powders, thermal history of annealing and

quenching treatment, and impact energy as a function of velocity for the impact ignition testing apparatus.

ACKNOWLEDGMENTS

The authors are grateful for support from ONR under contract (N00014-16-1-2079) managed by Dr. C. Bedford.

[1]V. I. Levitas, B. W. Asay, S. F. Son, and M. Pantoya, J. Appl. Phys. **101**, 083524 (2007).
[2]V. I. Levitas, Philos. Trans. R. Soc. A **371**, 20120215 (2013).
[3]V. I. Levitas, J. McCollum, and M. L. Pantoya, Sci. Rep. **5**, 7879 (2015).
[4]V. I. Levitas, B. Dikici, and M. L. Pantoya, Combust. Flame **158**, 1413 (2011).
[5]J. McCollum, D. K. Smith, K. J. Hill, M. L. Pantoya, J. Warzywoda, and N. Tamura, Combust. Flame **173**, 229 (2016).
[6]V. I. Levitas, J. McCollum, M. L. Pantoya, and N. Tamura, J. Appl. Phys. **118**, 094305 (2015).
[7]J. McCollum, M. L. Pantoya, and N. Tamura, Acta Mater. **103**, 495 (2016).
[8]V. I. Levitas, J. McCollum, M. L. Pantoya, and N. Tamura, Combust. Flame **170**, 30 (2016).
[9]K. L. McNesby, B. E. Homan, J. J. Ritter, Z. Quine, R. Z. Ehlers, and B. A. McAndrew, Propellants, Explos., Pyrotech. **35**, 57 (2010).
[10]J. L. Gottfried and E. J. Bukowski, Appl. Opt. **56**, 47 (2017).
[11]C. Capellos, E. L. Baker, S. Nicolich, W. Balas, J. Pincay, and L. I. Stiel, Shock Compression Condens. Matter **CP955**, 357 (2007).
[12]H. Wang, Y. Zheng, Q. Yu, Z. Liu, and W. Yu, J. Appl. Phys. **110**, 074904 (2011).
[13]A. Bachmair and R. Pippen, Mater. Sci. Eng., A **528**, 7589 (2011).
[14]E. M. Hunt, S. Malcolm, M. L. Pantoya, and F. Davis, Int. J. Impact Eng. **36**, 842 (2009).
[15]S. M. Walley, J. E. Balzer, W. G. Proud, and J. E. Field, Proc. R. Soc. A **456**, 1483 (2000).
[16]A. P. Hardt, in *Proceedings of the 13th International Pyrotechnics Seminar* (1988), p. 425.
[17]J. J. Davis and D. L. Woody, "Reactions in neat porous metal/metal and metal/metal oxide mixtures under shear induced plastic flow conditions," in *Metallurgical and Materials Applications of Shock-Wave and High-Strain-Rate Phenomena*, edited by L. E. Murr, K. P. Staudhammer, and M. A. Meyers (Elsevier, Amsterdam, 1995), pp. 661–668.
[18]Y. Wang, W. Jiang, X. Zhang, H. Liu, Y. Liu, and F. Li, Thermochim. Acta **512**, 233 (2011).
[19]B. A. Mason, L. J. Groven, and S. F. Son, J. Appl. Phys. **114**, 113501 (2013).
[20]A. G. Evans and J. W. Hutchinson, Int. J. Solids Struct. **20**, 455 (1984).
[21]G. Ligios, A. M. Bertetto, and F. Delogu, J. Alloys Compd. **554**, 426 (2013).
[22]S. M. Walley, J. E. Field, R. A. Biers, W. G. Proud, D. M. Williamson, and A. P. Jardine, Propellants, Explos., Pyrotech **40**, 351 (2015).
[23]W. L. Perry, J. A. Gunderson, M. M. Balkey, and P. M. Dickson, J. Appl. Phys. **108**, 084902 (2010).
[24]Y. Wu and F. Huang, Mech. Mater. **43**, 835 (2011).
[25]C. S. Coffey and V. F. DeVost, Propellants, Explos., Pyrotech. **20**, 105 (1995).
[26]M. Kunz, N. Tamura, K. Chen, A. A. MacDowell, R. S. Celestre, M. M. Church, and E. Ustundag, Rev. Sci. Instrum. **80**, 035108 (2009).
[27]V. I. Levitas, M. L. Pantoya, and B. Dikici, Appl. Phys. Lett. **92**, 011921 (2008).
[28]V. I. Levitas, M. L. Pantoya, and K. W. Watson, Appl. Phys. Lett. **92**, 201917 (2008).
[29]K. W. Watson, M. L. Pantoya, and V. I. Levitas, Combust. Flame **155**, 619–634 (2008).
[30]J. S. Wang and A. G. Evans, Acta. Mater. **46**, 4993 (1998).
[31]H. R. Le, M. P. F. Sutcliffe, P. Z. Wang, and G. T. Burstein, Acta Mater. **52**, 911 (2004).